Rotordynamic Analysis of 500 000 r/min 2 kW Ultra-High-Speed Machine for Portable Mechanical Antenna

Md Khurshedul Islam
Electrical and Computer Engineering
Mississippi State University
mi264@msstate.edu

Seundeog Choi
Electrical and Computer Engineering
Mississippi State University
seungdeog@ece.msstate.edu

***Abstract*— Bi-directional wireless communication between the earth's surface and underground or undersea facilities is infeasible because of the conventional electrical antenna's (CEA) excessive power requirement and enormous size. The most promising and power-efficient solution to this problem is using a mechanical-based antenna (AMEBA) that enables the ULF-VLF (0.03-10 kHz) communication in these conductive media. However, one of the main challenges in developing the AMEBA is designing its transmitter, i.e., the ultra-high-speed (UHS) rotor, which rotates the polarized permanent magnet (PPM) in a wide range of frequency. Because of the high rotating frequency and high load inertia of PPM, the UHS rotor's design becomes more critical in terms of Rotordynamic and vibration issues. This paper presents a detailed Rotordynamic analysis of a 2 kW, 500000 r/min UHS AMEBA rotor, which can generate transmitting frequency up to 8333 Hz. First, the UHS rotor's design is presented, which meets the torque and speed requirement of the AMEBA system. The impact of the different rotor materials on the rotor's undamped natural frequency is studied. Then, considering the AMEBA application, other rotor dynamic characteristics such as critical speed, bearing selection, Campbell diagram, and unbalance harmonic responses are investigated using 3-D finite element analysis (FEA). Finally, the UHS AMEBA rotor prototype is built, and an experiment of impulse hammer testing is performed to validate the rotor's undamped natural frequencies.**

Keywords—Ultra-high-speed machine, permanent magnet machine, Rotordynamic analysis, finite-element analysis (FEA), impulse hammer test, and mechanical-based antenna (AMEBA).

I. Introduction

In the trend of technology miniaturization, the use of ultra-high-speed machines (UHSM) is rapidly growing due to its attractive feature of low volume. The UHSM also offers several advantages, including high efficiency, compact structure, and high-power density [1-2]. As a result, UHSM is getting more and more attention, especially in high-tech industries such as robotics, portable power, and medicine [3-5]. Apart from these, one of the promising applications of UHSM is the rapidly growing wireless communication system [6-7]. With the current technology, wireless communication in the FR-denied environment (for example, communication between the earth's surface to the underground or deep seawater) is very limited in both distance and efficiency due to the high attenuation of these conductive media. The conventional coil antenna's lower field generation efficiency causes excessive input power [8] and requires a gigantic antenna that makes bi-directional communication impossible in the RF-denied media. One of the most promising and power-efficient solutions to this problem is using a mechanical-based antenna (AMEBA) system, which enables the possibility of underground and undersea communication by using extremely/very low frequency (0.03 to 10 kHz). It increases the skin depth of the electromagnetic waves that can penetrate a long distance in conductive environments. The AMEBA transmitter will significantly reduce the ULF/VLF communication system's antenna size and solve the excessive power requirement problem. Our previous work presents the working principle and efficiency of the AMEBA transmitter [9]. A simplified diagram of the AMEBA transmitter system is shown in Fig. 1, which includes a polarized permanent magnet (PPM) dipole, a UHS electrical motor, a power electronics interface, and a digital controller. Unlike a conventional electrical antenna, the mechanical antenna generates the oscillating magnetic field using the PPM, which consumes no power.

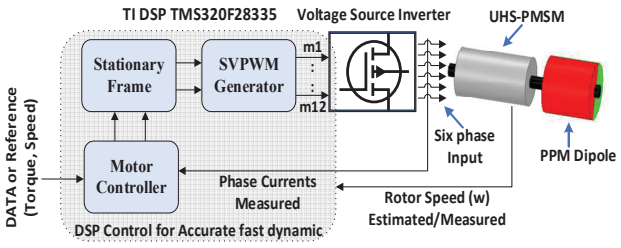

Fig. 1: Simplified diagram of a mechanically controlled antenna including UHS permanent magnet synchronous machine.

However, one of the critical challenges in developing this AMEBA is designing its mechanical transmitter, i.e., the UHS rotor, to drive the PPM at the transmitting frequency up to 10 kHz. Operating a rotor in this frequency range will encounter several critical bending frequencies. Usually, the UHS rotor does not operate at or close to its bending frequencies to avoid mechanical resonance [10], [11]. However, the AMEBA rotor cannot afford this flexibility because it will limit the antenna's communication bandwidth. Hence, the AMEBA rotor's design should avoid such bending frequencies to protect the transmitter from vibration leading to catastrophic failure. Another challenge in the design of the UHS AMEBA rotor is its unwanted vibration at the UHS operation. In the UHS machine, vibration can be generated from multiple sources, such as electromagnetic force, weak structural integrity, unbalance harmonic forces, inappropriate bearing selection, and improper crossing of the critical speed points. All the possible vibration sources and the maximum vibration limit should be investigated to avoid any mechanical breakdown. Hence, it is highly recommended to analyze the detailed Rotordynamic of the UHS AMEBA rotor during the design stage.

A review of Rotordynamic analysis, especially the critical speeds and vibration modes for rotating machinery, is presented in [12]. The Rotor dynamic and its experimental analysis of different high-speed rotors are reported in [13]-[14]. Studies have also investigated the Rotordynamic of UHS rotors having an operating speed of 500 r/min or more. However, its application and analysis for ULF/VLF communication systems have been limited. The critical speed, mode shape, and bearing selection of low power,

2021 IEEE International Electric Machines & Drives Conference (IEMDC) | 978-1-6654-0510-2/21/$31.00 ©2021 IEEE | DOI: 10.1109/IEMDC47953.2021.9449541

500000 r/min UHSM machine is presented in [15]. Besides PM machines, switched reluctance machine (SRM) is also studied for UHS operation. The Rotor dynamic analysis of a 100 W rotor for SRM has been presented in [16], which has a maximum rotational speed of 1.2 million r/min.

However, both rotors have very lower shaft torque at UHS operation, 1.9 mNm for [15] and 0.79 mNm for [16]. On the other hand, the UHS rotor of the AMBEA system requires a higher shaft torque at the UHS operation. In the studied AMEBA system, a hollow cylinder is considered, which has axial rotational inertia of 1.61×10^{-4} kg-m^2. Initially, the antenna is aimed to transmit a frequency of 0-8.3 kHz, which sets a rotational speed requirement of ~500000 r/min for a two-pole rotor. Considering the studied antenna's mechanical and communication requirements, a rotor is needed with a shaft torque of 38.2 mNm at 500000 r/min. Increasing the torque rating of a UHS rotor impels the rotor's axial length and outer diameter to a subtle limit, which leads the rotor to critical Rotordynamic and vibration issues. In literature, there is no previous work on the Rotordynamic analysis of the UHS rotor having a torque of 38.2 mNm at 500000 r/min. This paper presents the detailed rotor dynamic analysis of a unique UHS AMEBA rotor, which has a rated speed of 500000 r/min and rated power of 2 kW.

II. Rotor Geometry and Design

In an electric machine, the number of rotor poles (P) is related to the fundamental frequency (f) as $P= (120\times f)/Speed$. Hence, a 2-pole rotor is selected to minimize the high-frequency core loss and switching loss. The conventional rotor configuration is not suitable for UHS operation due to its excessive rotational speed. A simple and robust rotor configuration is desired for the UHS AMEBA rotor. The 2-D cross-sectional view and 3-D geometry of the studied AMEBA rotor are shown in Fig. 2. The rotor is composed of four parts: magnet, retaining sleeve and two shaft parts. In this rotor configuration, a cylindrical PM is buried inside the retaining sleeve, and the axial extension of the sleeve forms the rotor shaft. Unlike a conventional rotor geometry, the steel shaft is removed from the rotor center to use the maximum amount of PM, which increases the rotor's torque density significantly. This rotor configuration also benefits from the sinusoidal air-gap field, lower centrifugal force, lower air-friction loss, and smaller system volume, making it suitable for UHS rotor, especially when the rotational speed is more than 200000 r/min [15]-[17].

Considering the high centrifugal force and required high torque density, the optimal magnet radius is obtained as 3.9 mm. A 0.6 mm thick retaining sleeve is used on the rotor surface to prevent the magnet from scattering at UHS operation. The interference fit technique is used between the magnet and sleeve to ensure a rigid mechanical joint, essential for proper torque transfer from magnet to shaft. The shaft length depends on the rotor's stack length, bearing housing, and application requirement. However, the maximum shaft length of a UHS rotor is limited by the Rotor-dynamic constraint, i.e., the critical speed. Considering the electromagnetic and Rotordynamic constraints, the studied rotor has an optimal shaft length of 72 mm and an effective stack length of 40 mm, which is the axial magnet length.

A rare-earth magnet, Sm_2Co_{17}, is used in this rotor because of its outstanding thermal capability (operating temperature up to 350 °C) and higher electromagnetic energy

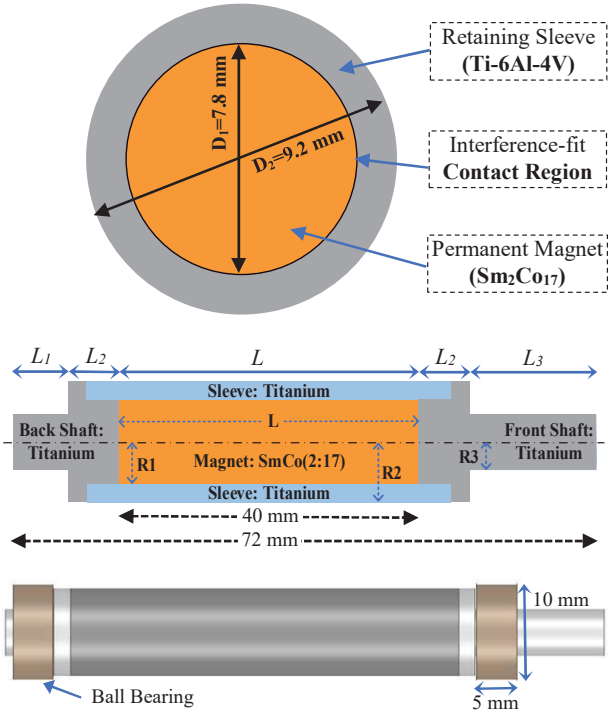

Fig. 2: 2-D cross section (top & middle), and side view (bottom) of the UHS AMEBA rotor.

density (BH_{max}) at high temperatures. However, the rear earth magnets are mechanically fragile, which needs a strong retaining sleeve to sustain against the high centrifugal force generated at UHS operation. Usually, the non-ferromagnetic material (for example, titanium alloy, stainless steel, and Inconel alloy having high tensile strength, good thermal conductivity, and lightweight are used as sleeve material. Besides, non-metallic wound material such as carbon fiber, glass fiber, and carbon-graphite is also a good option for the UHS rotor due to its lightweight and high mechanical strength. In this paper, both titanium alloy and carbon fiber are studied for Rotordynamic characteristics, and finally, the titanium alloy is selected for the prototype. The rotor shaft is also made of titanium alloy. A pair of customized ball bearing is used in the rotor, which has an inner ring diameter of 5 mm, outer ring diameter of 10 mm, and width of 5 mm. The selection of bearing is discussed in the next section.

III. Rotordynamic Analysis

In a high-speed rotor operation, any natural frequencies should be avoided before the fundamental operating frequency [18]. However, it is impossible for the UHS AMEBA rotor because of its high L/D ratio and lower stiffness value of the miniature bearing. For the reliable and efficient operation of the UHS AMEBA rotor, it is recommended to have an appropriate separation margin, at least 20 to 30%, between the natural frequencies and the fundamental operating frequency [19]. Also, considering the AMEBA transmitter's requirement, no natural frequency should occur in the lower speed region (< 180000 r/min) to ensure a wide bandwidth of the ultra-low frequency (ULF: 3 Hz to 3 kHz) communication.

The undamped natural frequencies (ω_n) of a cylindrical beam shaft made from a single material can be calculated using (1):

$$\omega_n = \alpha_n \sqrt{\frac{Er^2}{64\rho L^4}} \quad (1)$$

where E is Young's modulus and ρ is the mass density of the material, r is the radius and L is the length of the shaft, and α_n is a series constant of n_{th} natural frequency, which depends on the rotor's physical properties and boundary conditions. Equation (1) can be modified for the studied rotor geometry as (2):

$$\omega_n = \sqrt{\frac{(1/256)a_n^2 E R_2^4}{[\rho_{SL}\{R_s^2L_1^4+R_s^2L_3^4+2R_2^2L_2^4+(R_2-R_1)^2L^4\}+\rho_{PM}R_1^2L^4]}} \quad (2)$$

where R_1, R_2, R_3, L, L_1, L_2, and L_3 are rotor dimensions as shown in Fig. 2, ρ_{SL} and ρ_{PM} are the mass density of the sleeve and PM material, respectively. According to (2), one can be observed that as the shaft length increases, the value of rotor's natural frequencies decreases, which results in several critical speed points below or near the rated speed. This analytical equation is fast in calculation and also helps to better understand the effect of each rotor dimension, but it cannot calculate the rigid body frequencies and mode shapes. To do this, the finite element analysis (FEA) is also performed in this section using ANSYS workbench.

A. Undamped Natural Frequencies Analysis:

First, the undamped natural frequencies are calculated using both the analytical and FEA method. In this paper, a non-ferromagnetic material (titanium alloy) and a non-metallic material (carbon fiber) are studied as sleeve material to understand the variation of natural frequencies with respect to the material's mechanical properties. The titanium alloy is an isotropic material (having the same mechanical strength in all directions), but the carbon fiber is an orthotropic material (having different mechanical strength in the X and Z direction). The physical properties of all materials are given in table-I. The undamped natural frequency analysis results are shown in table-II, where the first two bending frequencies are calculated. In the case of titanium alloy, the first bending frequency (FBF) is above the rated frequency (8333 Hz) with a safety factor (SF) of 9%. Considering carbon fiber (strengthen in the X direction), the FBF falls below the rated frequency, which is not acceptable. On the other hand, the FBF is well above the rated frequency with an SF of 45% when the carbon fiber (strengthen in the Z direction) is applied. However, the carbon fiber material is not used in the AMEBA rotor because its maximum operating temperature is limited to 250°C, and it is not suitable for the interference-fit operation.

In addition to bending frequencies, the FEA model also presents the rigid body frequencies and mode shapes. In the FEA model, a 3-D rotor is considered, and a free-free boundary condition is applied. According to the simulation result, the first four natural frequencies are 1 Hz, 5 Hz, 9012 Hz, and 17053 Hz. Fig. 3 shows the AMEBA rotor's deformation modes at these frequencies. The first two lower frequencies are rigid body frequency, generating a lateral (1 Hz) mode shape and a conical (5 Hz) mode shape. On the other hand, the third and fourth frequencies generate the 1st (9012 Hz) and 2nd (17053 Hz) order bending mode shape.

Table-I: Mechanical properties of UHS rotor materials

Properties	Ti-6Al-4V	Carbon fiber	Sm_2Co_{17}
Density (kg/m^3)	4430	1490	8300
Young's Modulus (GPa)	114	120 (x) 8.6 (y & z)	104
Shear Modulus (GPa)	42	3.1 (yz) 4.7 (xy & xz)	40
Poisson's ratio	0.35	0.4 (yz) 0.27 (xy & xz)	0.28

Table - II: Undamped Natural frequency analysis result

Frequency	Analysis	Titanium	CF (X)*	CF (Z)*
1st order bending mode (Hz)	Analytical	9103	8402	12111
	FEA	9012	8316	12020
2nd order bending mode (Hz)	Analytical	17148	14107	210244
	FEA	17053	14020	210145

*CF(X) = Carbon fiber strengthen in X, CF(Z) = Carbon fiber strengthen in z direction

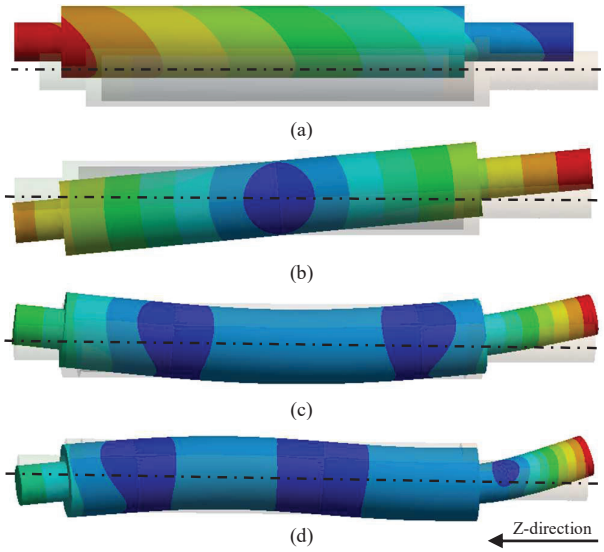

Fig. 3: Deformation mode shape of the AMEBA rotor at different undamped natural frequencies: (a) lateral mode (1 Hz), (b) conical mode (5 Hz), (c) 1st order bending mode (9012 Hz), and (d) 2nd order bending mode (17053 Hz).

B. Selection of Guide Bearing:

The use of guide bearings directly influences the undamped natural frequencies of the rotor. Fig. 4 shows the variation of the first four natural frequencies with the different bearing stiffness values. It is observed that the 1st lateral mode frequency increases as the bearing stiffness increases, but when the bearing stiffness reaches 100 MN/m, it is not changing anymore. A similar phenomenon is observed for 2nd, 3rd, and 4th natural frequency, but they are saturated at different bearing stiffness. It is worth mentioning that applying an excessive stiff guide bearing may lead the rotor to a serious 1st mode stability issue.

In the UHS machine, the design and selection of bearing depend on various factors such as the maximum operating speed, mechanical load characteristics, available bearing housing area, bearing loss, bearing temperature, operation hours, and bearing surrounding environment. In literature, three types of bearing are used in the UHS machine: ball bearing, air bearing, and magnetic bearing.

Ball bearings are always the first choice for a rotating machine because of their simplest design and high robustness. However, it causes high friction loss in the UHS operation. In literature, ball bearings are used in miniature machines with a rotating speed of 1 million r/min [4], though the maximum speed it reached is nearly 750000 r/min. Ceramic ball bearing is commercially used in low torque, 500000 r/min PM machine [15].

Air bearings are non-contact frictionless bearing, which uses air pressure to levitate the rotor. This bearing can operate at UHS with minimum friction losses, but the maximum speed is limited by the instability issue. In literature, an airfoil bearing is tested up to 700000 r/min by MiTi [20]. A dynamic air bearing is used in a switched reluctance machine, having 1.2 million r/min maximum speed [21]. However, air bearing has a very low stiffness value, and it requires additional infrastructure for the housing and air-supply. It increases the total shaft length, which affects the rotor's natural frequency significantly.

Magnetic bearing uses magnetic forces produced by the permanent magnet and copper windings to levitate the rotor. It is also a contactless bearing suitable for high-speed operation, but its use is limited due to additional control circuitry and complex feedback control. In [22], [23], the use of magnetic bearing is reported for UHS machines.

The miniature air bearings have a lower stiffness value around 1×10^6 N/m [16], the stiffness of magnetic-bearing depends on the tuning, and ball bearings have the highest stiffness value, approximately 1×10^7 N/m [4]. In this study, a pair of ball bearing is selected for the AMEBA rotor considering the robust operation, compact AMEBA transmitter, control complexity, and availability. The bearing has a radial stiffness value of 10.1×10^6 N/m for the studied AMEBA rotor.

C. Campbell Diagram Analysis:

After selecting the bearing stiffness value, the Campbell diagram of the studied rotor can be generated using ANSYS FEA. Fig. 5 shows the meshing and bearing placement of the 3-D rotor in the ANSYS Modal module. Fig. 7 shows the Campbell diagram of the studied rotor, considering the boundary condition, the bearing stiffness, the gyroscopic effect, and the rotational velocity effect. A synchronous whirl line is drawn in the diagram to obtain critical speed points. The intersection of the natural frequency curve and the synchronous line are defined as critical speed points (CSP). The first four critical speed points are indicated in the figure. Due to the implementation of guide bearing stiffness, the rigid body modes are moved from 1 Hz to 2806 Hz and 5 Hz to 5956 Hz. The first bending frequency is shifted from 9012 Hz to 11250 Hz, and the second bending is also shifted from 17015 Hz to 21003 Hz. Consequently, the rated speed point (500000 r/min or 8333 Hz) falls between the 2nd and 3rd critical speed points. However, there is a 28% separation margin (SM) between the 2nd critical speed point and rated speed. This is 35% between the 3rd critical speed point and the rated speed point. Also, the first critical speed point is at 2806 Hz, which ensures the wide bandwidth ULF communication of the AMEBA transmitter. Fig. 6 shows the mode shape of the UHS AMEBA rotor at these critical speeds. It is seen that the first two critical speed points are dominated by the bearing stiffness. Hence, the first two critical speed points can be adjusted as desire using the

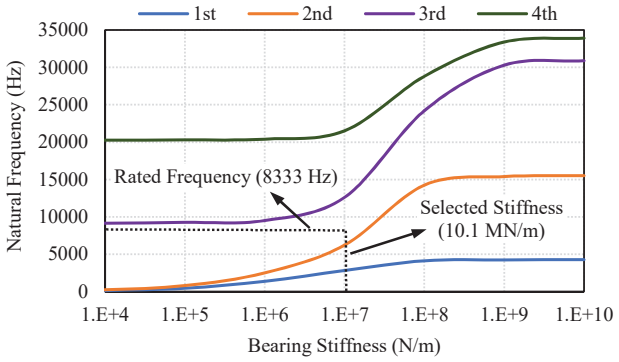

Fig. 4: Natural frequencies vs guide bearing stiffness.

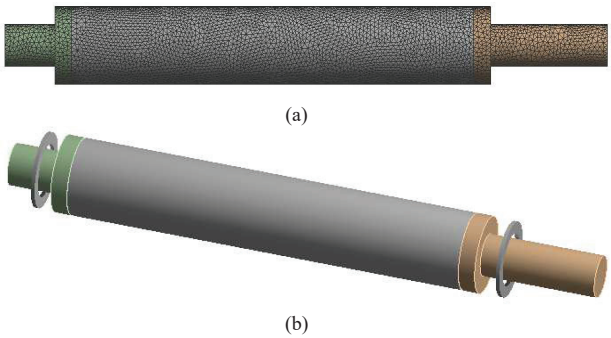

Fig. 5: 3-D FEA model for Campbell diagram analysis: (a) meshing (b) bearing installation.

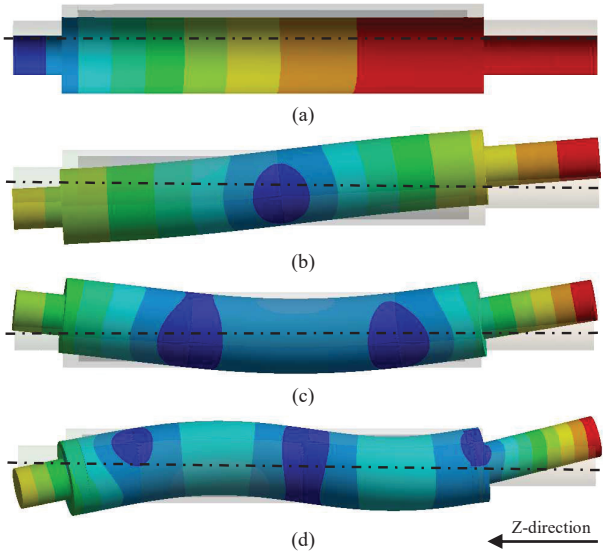

Fig. 6: Deformation mode shape of the AMEBA rotor at different critical frequencies: (a) lateral mode (2806 Hz), (b) conical mode (5956 Hz), (c) 1st order bending mode (11250 Hz), and (d) 2nd order bending mode (21003 Hz).

appropriate bearing stiffness. However, the bending frequencies are due to the rotor stiffness. Therefore, the rotor should never cross the bending frequencies to avoid any catastrophic failure or excessive vibration during the UHS operation.

With the increase of rotational speed, the applied gyroscopic moment weakens the system stiffness of the backward whirl (BW) and hardens the system stiffness of the forward whirl (FW), which splits each natural frequency into two modes (FW and BW). A high separation between the FW

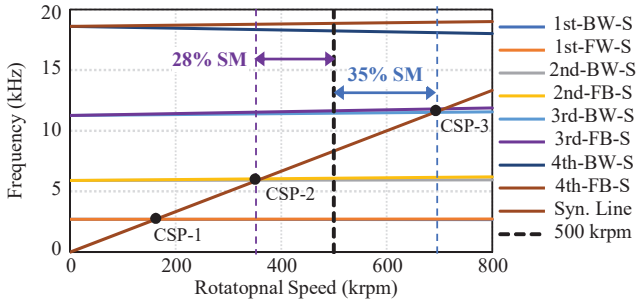

Fig. 7: Campbell diagram. [S-stable, US-unstable, CSP- critical speed point]

and BW is not accepted because it will limit the rotor's operation in between them. Fig. 7 also shows that all these modes are stable, and the difference between FW and BW mode of the first two critical frequencies is negligible, which confirms an excellent overall system stiffness and stability.

D. Unbalance Response Analysis:

In the UHS rotor, unbalance response analysis is essential to estimate the rotor's maximum deformation due to its unbalance characteristics. It is also important to ensure the minimum clearance in the air-gap between the stator and rotating rotor at the UHS operation. In this section, an unbalance response analysis of the AMEBA rotor is performed to estimate the maximum deformation or the vibration amplitude of the rotor due to its unbalance harmonic forces. The permissible residual unbalance (U_{max}) of the UHS rotor can be calculated by ISO-1940 standard [24] as (3):

$$U_{max} = 1000\left(\frac{G\times M}{N}\right) \quad \text{g.mm} \tag{3}$$

where G is the balance quality grade, which is 0.4 mm/s for the studied UHS rotor, M is the rotor mass (kg), and N is the rotational speed (rad/s). In this study, the first-order bending mode of the AMEBA rotor is considered for the unbalance response analysis because it is the nearest critical bending frequency point where the highest deformation has occurred. Fig. 8 shows the 1-D beam diagram of the 1st order bending mode shape and different observation point locations on the rotor. The calculated unbalance mass is applied on the 3rd point, which is the rotor center, as shown in the figure. Fig. 9 shows the frequency response function (FRF) result of the unbalanced response analysis at different rotor points. The acceptable vibration displacement (V_{allow}) of the AMEBA rotor can be roughly calculated using API-610 standard [25]

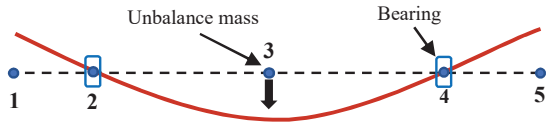

Fig. 8: 1st order bending frequency and different observation points for unbalance response analysis.

$$V_{allow} = 25.4\sqrt{(12000/n)} \tag{4}$$

as (4). Fig. 9 shows that, at the rated speed, both the rotor vibration level is well below the allowable limit (12.2 µm). Also, the rotor maintains the minimum clearance in the air-gap. However, at the 3rd and 4th critical speed, the vibration amplitude becomes excessively high (more than few millimeters), and the rotor fails to maintain the minimum mechanical clearance in the air-gap, which will result in a structural breakdown of the rotor. Hence, this AMEBA motor should never pass these critical bending frequencies (3r and 4th). The FRF result also shows that the vibration amplitude at the 1st and 2nd critical speed points reaches the allowable limit, but their restricted frequency bandwidth is very small. Therefore, the AMEBA rotor should not operate at these frequency bandwidths, and these frequencies should pass quickly and carefully during the continuous operation.

IV. Prototyping and Experimental Analysis

Due to the unconventional geometry, the development of USH rotor is different from the conventional rotor design process. This AMEBA rotor does not have any steel shaft through the rotor center, laminated rotor core, and any visible magnet. A miniature high-speed rotor can be developed using two process: 3-D printing or CNC machining technique. The additive manufacturing technique (AMT) is widely used for 3-D rotor printing. AMT has the advantage of easy prototyping, possible to design a complex geometry, and capable of rapid production. However, AMT is not suitable for the studied rotor prototyping, because AMT has a high dimension tolerance, which hinders the appropriate interference-fit implementation. A proper interference-fit between the magnet and sleeve is mandatory in the UHS AMEBA rotor to limit the PM stress and to ensure an efficient torque transfer from the magnet to the shaft. On the other hand, the CNC machining technique has a lower dimension tolerance, but it is comparatively cumbersome.

For the studied rotor, the titanium sleeve and shaft parts are designed using CNC machining technology and

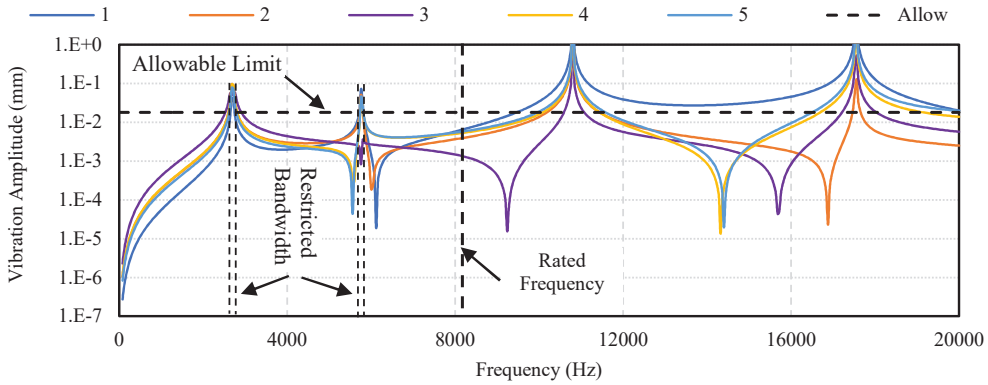

Fig. 9: Unbalance response analysis result: (Frequency Response Function).

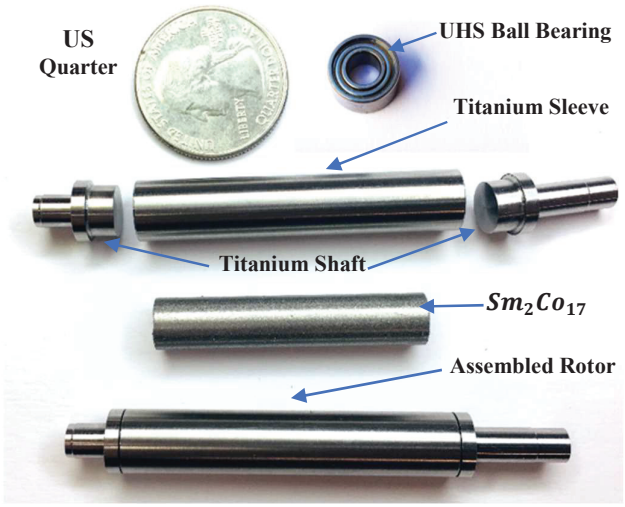

Fig. 10: UHS AMEBA rotor parts and assembly.

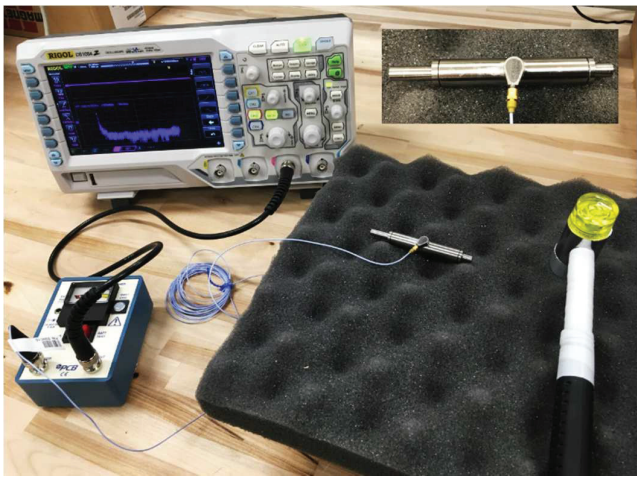

Fig. 11: Impact hammer test setup of UHS AMEBA rotor.

polishing. The designed parts have a precision tolerance of ± 0.005 mm. A pair of customized UHS ceramic ball bearing is used, which can operate at 500000 r/min continuously for at least 15 hours. Fig. 10 shows the rotor parts, the assembled rotor, and bearings of the AMEBA rotor. A 20 µm interference-fit is implemented between the magnet and sleeve using the shrink-fit technique. Besides, an adhesive is used in the joint of the shaft part and sleeve to improve the bonding. Finally, the rotor-balancing is done by scrubbing at different points on the rotor surface.

Accurate prediction of the AMEBA rotor's natural frequencies is crucial. Hence, an experimental modal analysis of the prototyped rotor is performed to accurately predict the AMEBA rotor's natural frequencies. The impulse hammer test technique is used in this study. Fig. 11 shows the impulse hammer test experimental setup of the assembled AMEBA rotor. In this experiment, a tip changeable impulse hammer is used to excite the rotor mechanically, and an IEPE acceleration sensor is used to measure the rotor's frequency response. The sensor has a measurement range up to ± 500 g (pk), broadband resolution of 0.004 g (RMS), and the frequency range from 1 to 20000 Hz. A signal-conditioner module is used to power the sensor. It also amplifies the sensor output and sends it to the oscilloscope. The sensor is attached to the rotor surface using quick bond gel and a low-

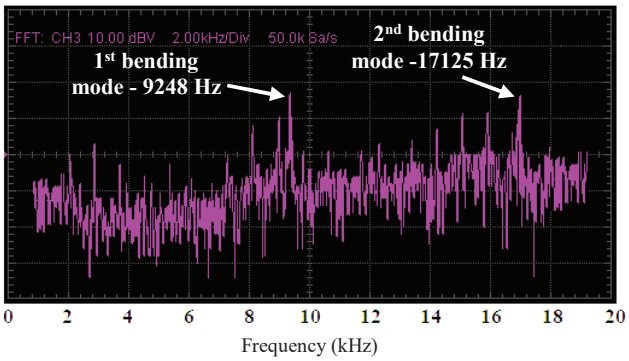

Fig. 12 Frequency spectrum of impulse hammer test.

attenuating non-stiff media supports the rotor. A one-side supported hanging rubber foam is used to ensure the undamped free-free boundary condition.

Fig. 12 shows the frequency response function of the assembled AMEBA rotor when the rotor is mechanically excited using the impulse hammer. The plot is obtained by performing FFT of the acceleration sensor's output signal. In this plot, the first two rigid body modes are not separable due to their low amplitude. However, two separable peaks are visible in the spectrum at 9248 Hz and 17125 Hz. These are the first and second-order bending modes, correspondingly. It is also observed that the experimental results have an excellent agreement with the FEA undamped natural frequency analysis results (section- IV(A)).

V. Conclusion

This paper presents the Rotordynamic analysis of a high-torque, ultra-high-speed PM rotor, having a rotational speed of 500000 r/min and a rated power of 2 kW. It will be used as a mechanical transmitter for ULF/VLF communication in the conductive media. The rotor uses an unconventional geometry where a cylindrical PM is buried inside the retaining sleeve and the axial extension of the sleeve forms the rotor shaft. The rear earth magnet, Sm_2Co_{17} is used as PM due to its outstanding electromagnetic and thermal characteristics. During the selection of sleeve material, the impact of different materials on the rotor's undamped natural frequency is observed. The carbon fiber (strengthen in the X direction) provides the maximum separation margin between the natural frequency and rated frequency. However, the titanium alloy is selected as sleeve material over the carbon fiber due to its higher operating temperature and shrink-fit implementation. Bearing selection and its impact on the rotor's critical speed points are discussed. The UHS ball bearing is selected for the studied rotor considering the required system damping, rotor robustness, and shaft length. The critical speed points and the rotor's deformation mode at these frequencies are analyzed using 3-D FEA. The rated speed falls between the 2nd and 3rd critical speed points with a minimum separation margin of 28%. The unbalance harmonic analysis result shows that the rotor's maximum vibration level at the rated speed is below the allowable limit. Also, the rotor maintains the minimum air-gap clearance throughout the full operating speed region. The experimental validation of the modal analysis is performed using impulse hammer test. The experimental result shows a good agreement with the FEA result with an error of 1.7%. Therefore, the rotor dynamic results confirm that the studied

UHS rotor is suitable for the effective and stable operation of the AMEBA transmitter.

ACKNOWLEDGMENT

This research was supported in part by the National Science Foundation CCSS-Comms Circuits &Sens System Program (Award Number 1905434).

Reference

[1] C. H. Park, S. K. Choi, and S. Y. Ham, "Design and experiment of 400,000 rpm high speed rotor and bearings for 500W class micro gas turbine generator," in *Proc. Int. Conf. Micro Nanotechnol. Power Gener.Energy Convers. Appl.*, Daejeon, 2011, pp. 1–4.

[2] J. Dang, S. Haghbin, Y. Du, C. Bednar, H. Liles, J. Restrepo*, et al.*, "Electromagnetic design considerations for a 50,000 rpm 1kW Switched Reluctance Machine using a flux bridge," in *Electric Machines & Drives Conference (IEMDC), 2013 IEEE International*, 2013, pp. 325-331.

[3] K. Isomura *et al.*, "Experimental verification of the feasibility of a 100Wclass micro-scale Gas turbine at an impeller diameter of 10 mm," *J. Micromech. Microeng.*, vol. 16, no. 9, pp. 254–261, Mar. 2006.

[4] C. Zwyssig, J. W. Kolar, and S. D. Round, "Megaspeed drive systems: Pushing beyond 1 million r/min," *IEEE/ASME Transactions on mechatronics,* vol. 14, pp. 564-574, 2009.

[5] D. Jung, J. Lee, J. Kim, I. S. Jang, J. Lee and H. Lee, "Design Method of an Ultrahigh Speed PM Motor/Generator for Electric-Turbo Compounding System," in IEEE Transactions on Applied Superconductivity, vol. 28, no. 3, pp. 1-4, April 2018, Art no. 5202804,

[6] M. T. B. Tarek, S. Dharmasena, A. Madanayake, S. Choi, J. Glickstein, J. Liang, and S. Mandal, ''Power-efficient data modulation for allmechanical ULF/VLF transmitters,'' in Proc. IEEE 61st Int. Midwest Symp. Circuits Syst. (MWSCAS), Aug. 2018, pp. 759–762.

[7] A. Madanayake, S. Choi, M. Tarek, S. Dharmasena, S. Mandal, J.Glickstein,andA.Sehirlioglu,''Energy-efficientULF/VLFtransmitters based on mechanically-rotating dipoles,'' in Proc. Moratuwa Eng. Res. Conf. (MERCon), May 2017, pp. 230–235.

[8] S. Gong, Y. Liu, and Y. Liu, "A Rotating-Magnet Based Mechanical Antenna (RMBMA) for ELF-ULF Wireless Communication," *Progress In Electromagnetics Research M*, Vol. 72, 125-133, 2018.

[9] J. S. Glickstein, J. Liang, S. Choi, A. Madanayake and S. Mandal, "Power-Efficient ELF Wireless Communications Using Electro-Mechanical Transmitters," in IEEE Access,vol. 8, pp. 2455-2471, 2020

[10] C. Gong, S. Li and T. G. Habetler, "Rotor Dynamic Analysis of Ultra-high Speed Switched Reluctance Machines over 1 Million rpm," 2018 IEEE Energy Conversion Congress and Exposition (ECCE), Portland, OR, USA, 2018, pp. 1704-1709.

[11] J. D. Ede, Z. Q. Zhu and D. Howe, "Rotor resonances of high-speed permanent-magnet brushless machines," in IEEE Transactions on Industry Applications, vol. 38, no. 6, pp. 1542-1548, Nov.-Dec. 2002.

[12] E. Swanson, C.D. Powell and S. Weissman, "A practical review of rotating machinery critical speeds and modes", *Sound and vibration*, vol. 39, pp. 16-17, 2005.

[13] J.D. Ede, Z. Zhu and D. Howe, "Rotor resonances of high-speed permanent-magnet brushless machines", *IEEE Transactions on Industry Applications*, vol. 38, pp. 1542-1548, 2002.

[14] H.-W. Cho, K.-J. Ko, J.-Y. Choi, H.-J. Shin and S.-M. Jang, "Rotor natural frequency in high-speed permanent-magnet synchronous motor for turbo-compressor application", *IEEE Transactions on Magnetics*, vol. 47, pp. 4258-4261, 2011.

[15] C. Zwyssig, J. Kolar, W. Thaler and M. Vohrer, "Design of a 100 W 500000 rpm permanent-magnet generator for mesoscale gas turbines", *Fourtieth IAS Annual Meeting. Conference Record of the 2005 Industry Applications Conference 2005*, pp. 253-260, 2005.

[16] C. Gong, S. Li and T. G. Habetler, "Rotor Dynamic Analysis of Ultra-high Speed Switched Reluctance Machines over 1 Million rpm," *2018 IEEE Energy Conversion Congress and Exposition (ECCE)*, Portland, OR, USA, 2018, pp. 1704-1709.

[17] N. Uzhegov, E. Kurvinen, J. Nerg, J. Pyrhönen, J. T. Sopanen and S. Shirinskii, "Multidisciplinary Design Process of a 6-Slot 2-Pole High-Speed Permanent-Magnet Synchronous Machine," in IEEE Transactions on Industrial Electronics, vol. 63, no. 2, pp. 784-795, Feb. 2016.

[18] P. Pfister and Y. Perriard, "Very-High-Speed Slotless Permanent-Magnet Motors: Analytical Modeling, Optimization, Design, and Torque Measurement Methods," in IEEE Transactions on Industrial Electronics, vol. 57, no. 1, pp. 296-303, Jan. 2010.

[19] Hong, Do-Kwan et al. "Unbalance response analysis and experimental validation of an ultra high speed motor-generator for microturbine generators considering balancing." *Sensors (Basel, Switzerland)* vol. 14,9 16117-27. 29 Aug. 2014.

[20] M. Salehi, H. Heshmat, J. F. Walton II, and M. Tomaszewski, "Operation of a mesoscopic gas turbine simulator at speeds in excess of 700,000 rpm on foil bearings," Proc. ASME Turbo Expo 2004, Power for Land, Sea, and Air, Vienna, Austria, June 14-17, 2004, Paper GT2004-53870.

[21] C. Gong, S. Li and T. Habetler, "High-Strength Rotor Design for Ultra-High Speed Switched Reluctance Machines," in IEEE Transactions on Industry Applications, vol. 56, no. 2, pp. 1432-1442, March-April 2020.

[22] A. Looser and J. W. Kolar, "An active magnetic damper concept for stabilization of gas bearings in high-speed permanent-magnet machines," *IEEE Transactions on Industrial Electronics,* vol. 61, pp. 3089-3098, 2014.

[23] S. Li, Y. Li, W. Choi, and B. Sarlioglu, "High-speed electric machines: Challenges and design considerations," *IEEE Transactions on Transportation Electrification,* vol. 2, pp. 2-13, 2016.

[24] ISO 1940-1, Mechanical vibration – balance quality requirements of rigid rotors – part 1 : determination of permissible residual unbalance.

[25] API Standard 611, General-purpose steam turbines for petroleum, chemical, and gas industry services, fifth edition, Washington, D.C. (2004).